Colloids and Surfaces A: Physicochem. Eng. Aspects 449 (2014) 121–128

Contents lists available at ScienceDirect

Colloids and Surfaces A: Physicochemical and Engineering Aspects

journal homepage: www.elsevier.com/locate/colsurfa

Adsorption of picloram herbicide on montmorillonite: Kinetic and equilibrium studies

Jose L. Marco-Brown[a], María M. Areco[a], Rosa M. Torres Sánchez[b], María dos Santos Afonso[a,*]

[a] Departamento de Química Inorgánica, Analítica y Química Física (DQIAQF) e Instituto de Química Física de los Materiales, Ambiente y Energía (INQUIMAE), Facultad de Ciencias Exactas y Naturales (FCEyN), Universidad de Buenos Aires (UBA), Ciudad Universitaria, Pabellón II, C1428EHA Buenos Aires, Argentina

[b] Centro de Tecnología en Minerales y Cerámica (CETMIC) – Camino Centenario y 506 CC (49), B1897ZCA M. B. Gonnet, Argentina

HIGHLIGHTS

- The kinetics of the adsorption of picloram onto montmorillonite was studied in situ by ATR-FTIR.
- A mixed surface reaction intra-particle diffusion-control was the kinetic model that best represented the results.
- The adsorption equilibrium isotherms were obtained at pH values of 3, 5 and 7.
- Two independent adsorption processes on different surface sites were found.
- The interaction of picloram with montmorillonite surface was confirmed by ATR-FTIR.

GRAPHICAL ABSTRACT

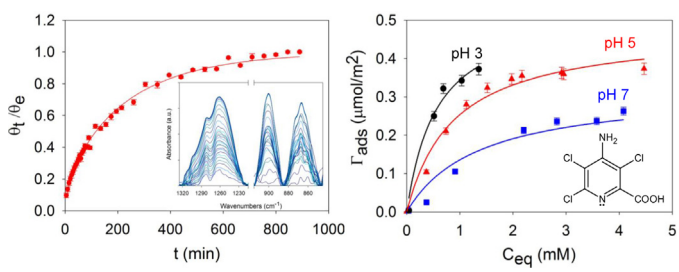

ARTICLE INFO

Article history:
Received 9 December 2013
Received in revised form 12 February 2014
Accepted 13 February 2014
Available online 22 February 2014

Keywords:
Picloram
Herbicide
Montmorillonite
Adsorption isotherms
Adsorption kinetics

ABSTRACT

The kinetics of the adsorption of picloram (PCM) onto montmorillonite (Mt) was studied in situ by attenuated total reflectance Fourier-transform infrared spectra (ATR-FTIR). Pseudo-first-order, pseudo-second-order, intra-particle diffusion and mixed surface reaction intra-particle diffusion-controlled kinetic models were applied to the experimental results. The latter was the model that best represented the experimental results. The adsorption equilibrium isotherms revealed the presence of two independent adsorption processes on different surface sites. The adsorption isotherms normalized by the surface area were fitted with the Langmuir and Freundlich models to obtain the respective parameters.

Due to the anionic form of PCM, the adsorption onto the external clay mineral surface sites followed by the entrance of the PCM molecule into the Mt basal space in a less energetically favorable pathway was proposed. The interaction of PCM with montmorillonite surface sites through nitrogen of the pyridine ring and carboxylic group by forming an inner sphere complex was confirmed by ATR-FTIR.

Abbreviations: ATR, Attenuated total reflectance; C.A., chemical analysis; CEC, cation exchange capacity; EDS, energy-dispersive X-ray spectroscopy; FTIR, Fourier-transform infrared spectra; IEP_{pH}, isoelectric point; rh, relative humidity; SEM, scanning electron microscopy; S_I, interlayer surface area; S_{N2}, external specific surface area determined by nitrogen adsorption; S_w, total specific surface area determined by water adsorption; XRD, X-ray diffraction analysis.

* Corresponding author. Tel.: +54 11 4576 3378/80ext125; fax: +54 11 4576 3341.
E-mail addresses: dosantos@qi.fcen.uba.ar, mdsafonso@gmail.com (M. dos Santos Afonso).

http://dx.doi.org/10.1016/j.colsurfa.2014.02.038
0927-7757/

1. Introduction

Due to the large-scale use of agricultural chemicals, synthetic organic pollutants are present in natural waters worldwide, and even water pollution accidents by organic chemicals are frequently reported [1].

The behavior of these synthetic organic chemicals in the environment is a dynamic phenomenon and detailed information about the chemical reaction remains deficient. These chemicals can reach wells, streams, rivers and lakes [2] or leach through the soil with the ability to reach and contaminate groundwaters [3,4]. Among the agrochemicals in use today, picloram, 4-amino-3,5,6-trichloropyridine-2-carboxylic acid (PCM), is a synthetic organic chemical that belongs to the pyridine family. This organic compound has herbicide activity and is used to control annual broadleaf weeds at low rates and deeply rooted herbaceous weeds, vines and woody plants at higher rates in cereals such as wheat, barley, sugarcane and oats [2,5].

Picloram has been detected in soils and fresh water [2,6]. PCM has an anionic character at the pH of most soils and water environments ($pK_a \approx 2.3$), which causes its sorption onto soil particles to be very low. Consequently, PCM has extremely high soil mobility and therefore, PCM has been classified as a pesticide with a high leaching potential [7–12].

The adsorption of herbicides onto solid adsorbents is very important, since it can effectively remove pollutants from aqueous streams [13–15]. Within the adsorbent materials studied to address the purification of polluted water, low-cost materials, such as clays, have revealed for PCM very low adsorption efficiency, while better adsorption efficiency was found for hydrotalcite [15], silica gel [16] or iron-pillared clay [17], and a direct relation was found between PCM adsorption and organic matter [8,18,19]. Within soils the adsorption of pesticides often involves the binding of positively charged pesticide molecules to the negatively charged components: organic matter and clay particles. Being both organic matter and clay materials reported as good adsorbents for nonionic pesticides [20,21].

Montmorillonite (Mt), which is a member of the smectite clay family, has been primarily selected to evaluate the sorption of different pesticides [22], heavy metals ions [23] or organic compounds [24] because of its high cationic exchange capacity (CEC) and specific surface area.

Previous studies have been conducted using Mt or modified Mt (e.g. its calcined form) to adsorb the cationic pesticides thiabendazole and benzimidazole [25,26], and the zwitterion glyphosate ([27] – and references cited therein). Those studies allowed to determine the main adsorption mechanism involved as cation exchange or monodentate or bidentate complexes formation kinetic studies of organic adsorbents on montmorillonite are only realized, up to our knowledge, with insecticides [27], and dyes [28].

The Attenuated Total Reflectance Fourier Transform Infrared (ATR-FTIR) spectroscopy has been successfully used in kinetic studies of adsorption involving anions on different solids [29] and can give a clearer understanding of the behavior of Picloram adsorbed in Montmorillonite.

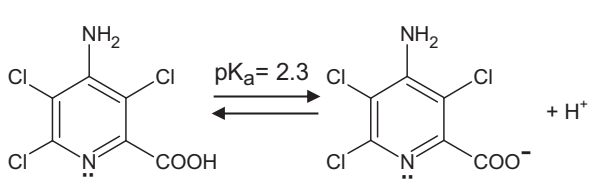

Fig. 1. Structural formula of picloram.

The aim of this work is to study the adsorption of PCM onto Mt and to understand the adsorption mechanism by in situ kinetic study using ATR-FTIR method. Both results could contribute to the understanding of the reactions at the clay mineral interface and will assist in predicting the mobility, fate and bioavailability of these pesticides in soil systems with a low percentage or without interactions among all components.

2. Experimental

2.1. Materials

Analytical PCM (Fig. 1), which had a purity of 100%, solubility in water of 1.78 mM for pH 3 and 5.0 mM for pH values of 5, and 7, and a $pK_a = 2.3$ [15], was supplied by Sigma–Aldrich Co. and used as received. All of the other chemical reagents were provided by Merck PA and used without any further purification. Water was purified using a Milli-Q system from Millipore Inc.

Montmorillonite API # 26, Clay Spur, Wyoming, was provided by Ward's Natural Science Establishment, Inc., USA. This Mt was manually milled in an agate mortar and sieved to a particle size of less than 125 μm.

2.2. Characterization of the adsorbent

The main properties of Montmorillonite API #26, reported in previous work [30], were a cation exchange capacity (CEC) of 138 meq/100 g determined using the formaldehyde method [30], purity >98% determined by X-ray diffraction (XRD), and an isoelectric point (IEP_{pH}) at pH 3.2 determined by the diffusion potential method [31]. The chemical composition and isomorphic substitutions of Mt were determined from the chemical analysis using the method reported by Siguin et al. [32].

The elemental composition of the Mt was determined using chemical (C.A.) and surface chemical analyses by energy-dispersive X-ray spectroscopy (EDS).

Scanning electron microscopy (SEM) was performed using a field emission gun scanning electron microscope Zeiss (FEG-SEM Zeiss LEO 982 GEMINI) coupled with an energy dispersive X-ray analyzer (EDS), which provides the qualitative and semiquantitative composition of the sample. The SEM images were collected by applying a 5 kV voltage with different magnifications to clarify the surface. The Mt sample was fixed to 10 mm metal mounts using carbon tape and sputter-coated with gold under vacuum in an argon atmosphere. The INCA software package was used to determine the elemental composition of the surface of the sample.

The total specific surface area was determined from the water adsorption (S_w) at room temperature and a relative humidity of 56% and external specific surface area by nitrogen adsorption (S_{N2}) at 77 K on samples that were previously dried at 100 °C for 6 h under high vacuum using a Micromeritics Accusorb 2100 E instrument. The internal or interlayer surface area (S_I) was calculated as the difference between total and external specific surface areas, S_w and S_{N2}, respectively.

2.3. Adsorption kinetics

The attenuated total reflectance Fourier transform infrared spectra (ATR-FTIR) were performed in a Nicolet 8700 FTIR spectrometer (200 scans, resolution 4 cm^{-1}) equipped with a liquid N_2 cooled MCT-A detector and a Spectra Tech ZnSe–ATR crystal unit (area = 10 mm × 72 mm) with an incident angle of 45° and 11 reflections.

A thin colloidal film of Mt was deposited onto an ATR crystal by placing 1.0 mL of Mt dispersion (0.8 g L^{-1}, pH 5) and evaporating to dryness at room temperature. The Mt film formed was rinsed with small aliquots of water to eliminate loosely deposited particles.

A volume of 1.5 mL of 5.0 mM of PCM fresh solution at constant ionic strength of 10.0 mM KCl, and pH 5 was placed on the Mt film. ATR-FTIR spectra were recorded as a function of time at room temperature until no further changes were detected. This indicated that the surface film had been saturated with the adsorbate. Typically, equilibration times were on the order of 890 min (~15 h). Temporal changes were estimated using the area under the curve for each selected frequency. These temporal changes were normalized by dividing the band area by the band area at equilibrium time. A baseline correction was made for instrumental instabilities and the background was subtracted. The spectra of the Mt film and PCM solution were previously recorded.

2.4. Adsorption experiments

The adsorption isotherms of PCM in Mt dispersions of 16 g L^{-1} were obtained using batch equilibration experiments at pH values ranging from 3 to 7 and initial concentrations of PCM ($C_{0,PCM}$) ranging from 0.04 to 5.0 mM at a constant ionic strength (1.0 mM KCl). The dispersions were shaken and equilibrated for 48 h at room temperature, and the pH was adjusted several times to maintain the respective values (3, 5 or 7) using drops of HCl or KOH aqueous solutions of different concentrations selected to avoid dilution. The $C_{0,PCM}$ maximum concentration used was established by the low solubility of PCM. The control samples, which did not contain PCM, were prepared using the same procedure.

The supernatant solutions were subsequently filtered through 0.22 μm cellulose nitrate membranes, and the concentration of PCM was determined using ion chromatography with a DIONEX DX-100 instrument equipped with a conductivity detector, a manual sample injection valve, and a 25 μL sample loop. Two plastic anion columns, DIONEX AG-4 and AS-4, were coupled in series to serve as the pre-column and the analytical chromatographic column, respectively. A mixture of 4.25 mM/4.50 mM HCO_3/CO_3^{2-} was used as the eluent at a flow rate of 2 mL min^{-1}. The retention time of PCM under these experimental conditions was 3.2 min. The amount of PCM adsorbed was determined as the difference between the initial concentration and that of the PCM in equilibrium with the supernatant.

The solute concentration (C_{eq}) in the supernatant of the Mt samples determined using ion chromatography was higher than the initial one because a concentration effect of the adsorbate in the solution occurs due to the amount of water incorporated during the swelling of the clay mineral. The wetting and drying processes linked to the clay mineral swelling have a volume (or mass) change associated. To account for this effect, the amount of incorporated water was determined from the mass difference between the dry clay mineral and some PCM pellet samples centrifugated at 17,000 rpm. Thereafter, the solution supernatant volume and PCM concentration at equilibrium was recalculated.

Furthermore, the surface coverage (Γ_{ads}) was calculated by normalizing the adsorbed amount of PCM by mass or area units (μmol g^{-1} or μmol m^{-2}).

2.5. Reproducibility and data analysis

All experiments were carried out by duplicate. Unless otherwise indicated, all data shown are the mean values from two replicate experiments. Standard deviations were below 5% in all cases.

The statistical data analysis was done using the SigmaPlot software package. SigmaPlot uses the Durbin–Watson statistic to test residuals for their independence of each other. The Durbin–Watson statistic is a measure of serial correlation between the residuals. The residuals are often correlated when the independent variable is time and the deviation between the observation and the regression line at a given time is related to the deviation at the previous time.

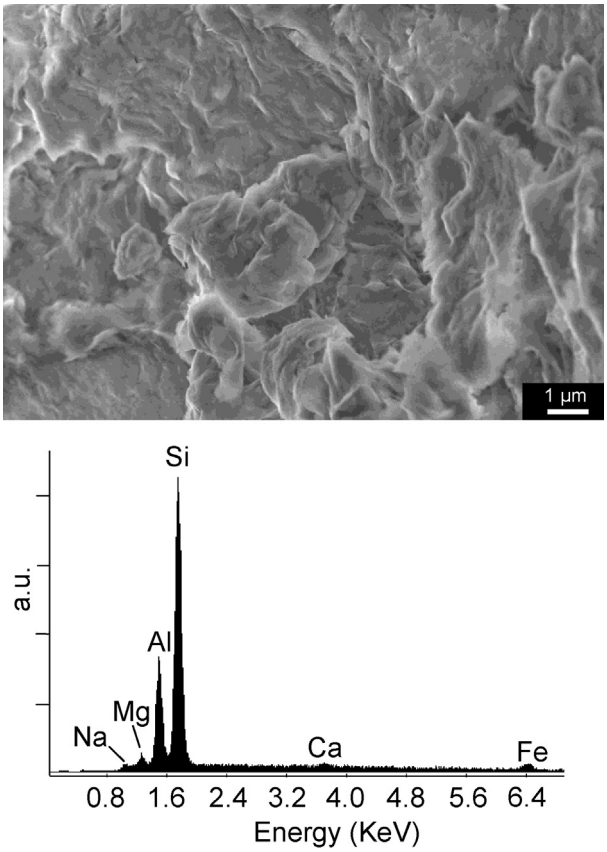

Fig. 2. SEM and EDS analyses of Mt.

3. Results and discussion

3.1. Sample characterization

The SEM image of Mt (Fig. 2) revealed a face-to-edge contact between the particles with a random orientation, and no formation of domains (group of particles that act as a unit) or clusters (group of domains that act as a unit) was observed within the bulk clay mineral. However, agglomerates were identified in the SEM image.

The elemental compositions of the Mt sample determined by C.A. and EDS, expressed as percentage of oxides, are summarized in Table 1. There were no significant differences between the compositions determined using either analytical method. Therefore, the structural chemical formula including isomorphic substitutions of the Mt sample obtained from the C.A. results [32] was $[(Si_{3.94}Al_{0.06})(Al_{1.56}Fe_{0.18}Mg_{0.26})O_{10}(OH)_2]M^+_{0.32}$.

The specific surface area determined by N_2 adsorption measurements is commonly used for the characterization of adsorbent materials, oxides and soils (Table 1). In the case of microporous materials, the BET surface area describes the adsorption on the external surface particles and the condensation into the micropores [33]. Specific interactions with the polar surface sites can occur when nitrogen is used as a probe molecule. Therefore, quantifying the total specific surface area of clay minerals is not a simple procedure, and nitrogen may not be the best probe molecule for this purpose. Thus, the total surface area of Mt can be better attained by the adsorption of a polar molecule, such as water, alcohols, etc. [33]. The selection of the probe molecule will depend on the initial state, the nature of the interlayer cations, etc. Therefore, the

Table 1
Oxides content of Mt sample determined by C.A. and EDS expressed as percentage.

	SiO_2	Al_2O_3	Fe_2O_3	CaO	MgO	Na_2O	K_2O	TiO_2
C.A.	65.6 ± 0.1	23.1 ± 0.1	4.0 ± 0.1	1.0 ± 0.1	2.9 ± 0.1	2.8 ± 0.1	0.5 ± 0.1	0.2 ± 0.1
EDS	61.0 ± 0.5	19.0 ± 0.3	8.0 ± 0.4	1.4 ± 0.3	3.6 ± 0.4	2.7 ± 0.7	1.2 ± 0.1	1.8 ± 0.2

specific surface areas, determined from the adsorption of water and nitrogen, for the Mt sample represent the total and the external specific surface area, respectively, and the difference between both of them corresponds to the internal specific surface area.

The following values were determined for Mt: $S_W = 632 \pm 5\,m^2\,g^{-1}$, $S_{N2} = 27 \pm 5\,m^2\,g^{-1}$ and $S_I = S_W - S_{N2} = 605 \pm 5\,m^2\,g^{-1}$.

The value of S_{N2} for Mt agrees with values obtained by other authors [34]. The S_W values were 10 times greater than those of S_{N2}, which is in agreement with the swelling capacity of Mt [35].

3.2. FTIR spectra

ATR-FTIR spectra for PCM, Mt film and PCM-Mt are shown in Fig. 3A and B and Fig. S1. The band at 1362 cm^{-1}, which corresponds to symmetric stretching vibration ν_s of the dissociated carboxyl group of PCM in solution, remains constant along the time (the variation in the area value is less than 5%). The band at 1281 cm^{-1} is assigned to pyridine in-plane deformation δ(CH), while the band at 1265 cm^{-1} is assigned to pyridine ν(CC, CN) of the PCM molecule. The last band frequency shift from 1265 to 1261 cm^{-1} on the PCM-Mt spectra since PCM is coordinated with aluminol or silanol surface sites of Mt through nitrogen of the pyridine ring and carboxylic group [17,36]. Bands centered at 874 cm^{-1} and 849 cm^{-1} of PCM spectra are attributed to pyridine out-of-plane deformation, γ(CH) and carboxylate δ(CO_2), respectively, and shift to 900 cm^{-1} and 867 cm^{-1} on PCM-Mt spectra. These frequency shifts observed (26 and 18 cm^{-1}, respectively) could be attributed to changes on the symmetry of the molecular atoms that change their coordinative surroundings due to the interaction of PCM with the aluminol and/or silanol groups of the solid surface. This suggests the formation of an inner sphere surface complex that involves chemical surface bonds while the outer sphere complexes retain their waters of hydration without changes in their symmetry.

The surface complexation occurs by COO^- group and nitrogen of the pyridine ring coordination to the surface as was previously suggested for PCM interaction with iron oxide pillared montmorillonite [17] and for picolinic acid interactions with Al(III)–(hydr)oxide minerals [36]. The formed inner-sphere surface complexes could be monodentate or bidentate complexes.

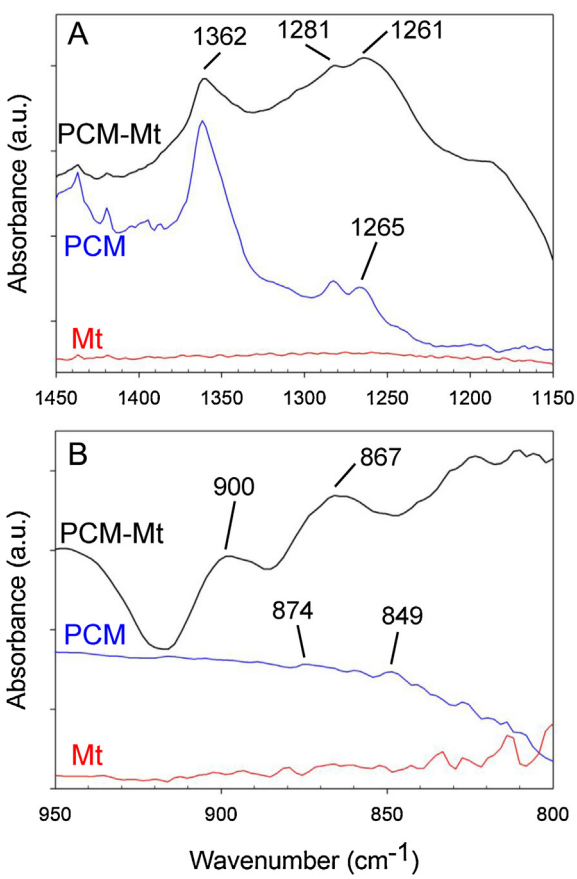

Fig. 3. ATR-FTIR spectra for Mt film, PCM solution and PCM adsorption on Mt film at t = 890 min, at pH 5 and room temperature. (A) Spectral range from 1450 to 1150 cm^{-1}. (B) Spectral range from 950 to 800 cm^{-1}.

3.3. Kinetics

Peaks centered at 1261, 900 and 867 cm^{-1} were used to follow the kinetic adsorption of PCM on Mt. The corresponding bands vary monotonously, without changes in their shape; thus, no indication of possible accumulation of intermediates was given by the spectral data. A typical time evolution of the bands centered at 1261, 900 and 867 cm^{-1} used for the kinetic adsorption experiment is shown in Fig. 4.

The time evolution of the band area centered at 900 cm^{-1} is shown in Fig. 5. This band area is directly related to the degree of surface coverage, θ_t. Therefore, this figure shows the surface coverage normalized by the surface coverage at equilibrium time θ_e with the time evolution. Bands centered at 1261 and 867 cm^{-1} time evolution are shown in Fig. S2.

The time evolution of θ_t/θ_e was found to be very reproducible, although the adsorption capacity showed rather large variations in the individual experiments.

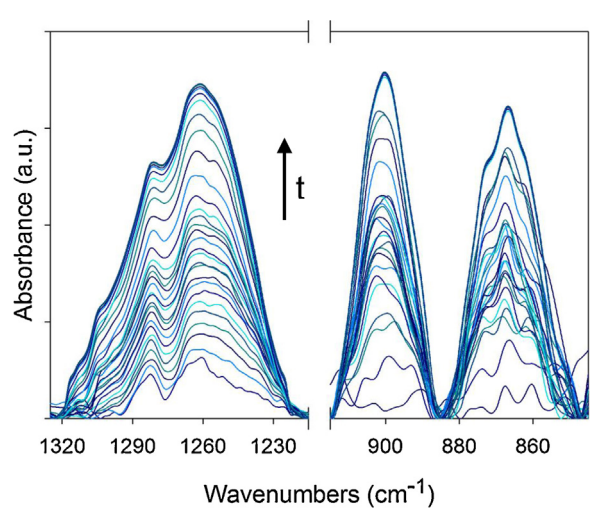

Fig. 4. ATR-FTIR time evolution of the bands centered at 1261, 900 and 867 cm^{-1} for kinetic adsorption experiment at pH 5 and room temperature.

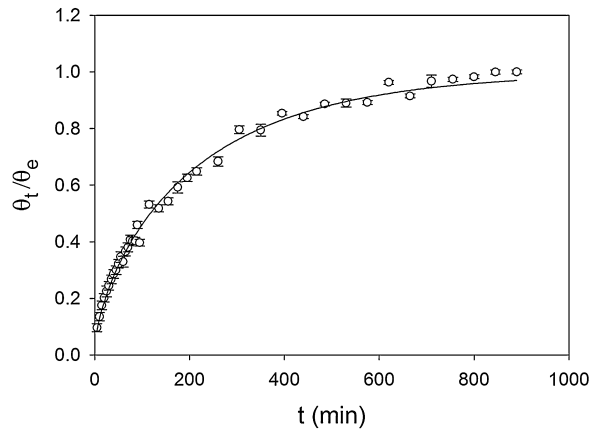

Fig. 5. Time evolution of the surface coverage, θ_t/θ_e, measured as the ATR-FTIR band area centered at 900 cm^{-1}, at pH 5 and room temperature. The solid line was obtained from Eq. (6) (MSR/DCK model).

Several kinetic models including Lagergren pseudo-first-order, pseudo-second-order, intraparticle diffusion models ([37,38] and references cited therein) and the mixed surface reaction and diffusion-controlled adsorption kinetic model recently proposed by Haerifar and Azizian [37] were tested for simulation of the experimental data.

3.3.1. Kinetic models

Adsorption kinetic data on different sorption systems were simulated using a variety of kinetic equations and models. Pseudo-first-order (PFO) and pseudo-second-order (PSO) equations and the intraparticle diffusion model (IDM) are the most widely used in the literature.

IDM is applicable when the rate-determining step is the mass transfer of adsorbate to the solid surface sites, while the other ones are used for modeling adsorption kinetics when the overall sorption rate is controlled by the rate of surface reaction.

The mixed surface reaction and diffusion-controlled adsorption kinetic model has been recently proposed by Haerifar and Azizian [37] for modeling adsorption kinetics when both diffusion and surface reaction steps control the overall rate of the process at the solid/solution interface.

3.3.1.1. Pseudo-first-order equation (PFO). The reversible PFO equation [39], widely used for biosorption, is based on a Lagergren pseudo-first-order rate expression:

$$\ln(\theta_e - \theta_t) = \ln\theta_e - k_1 t \tag{1}$$

where k_1 is the pseudo-first-order sorption rate constant, θ_e is the amount of PCM adsorbed at equilibrium by Mt and θ_t is the amount of PCM adsorbed at any time t. As mentioned before, θ_e and θ_t were measured as the area of bands centered at 1261, 900 and 867 cm^{-1}. The overall rate constant k_1 (Table 2), in min^{-1}, was calculated from the slope by plotting $\ln(1 - \frac{\theta_t}{\theta_e})$ versus t (Fig. S3). The determination coefficients obtained using the Lagergren model for the evaluated bands were lower than 0.95.

3.3.2. Pseudo-second-order equation (PSO)

This model assumes that the adsorption rate is proportional to the square of the number of unoccupied surface sites. Moreover, the number of occupied sites is proportional to the adsorbate concentration. This model is represented by Eq. (2) [38,39]:

$$\frac{d\theta_t}{dt} = k_2(\theta_e - \theta_t)^2 \tag{2}$$

Table 2
Parameters obtained for kinetics models.

		1261 cm^{-1}	900 cm^{-1}	867 cm^{-1}
PFO	k_1 (min^{-1}) × 10^3	5.6 ± 0.3	5.2 ± 0.3	4.1 ± 0.2
	R^2	0.9465	0.8638	0.8755
PSO	$k_2\theta_e$ (min^{-1}) × 10^3	8.2 ± 0.2	8.8 ± 0.1	9.4 ± 0.3
	R^2	0.9961	0.9926	0.9915
IDM	$k_{id}\theta_e^{-1}$ (min$^{-1/2}$) × 10^2	3.6 ± 0.1	3.4 ± 0.1	3.2 ± 0.1
	R^2	0.9519	0.9697	0.9637
MSR/DCK	u_{eq} × 10^{10}	1.1 ± 0.2	5.8 ± 0.1	5.0 ± 0.4
	k (mol^{-1} cm^3 min^{-1})	0.56 ± 0.03	0.84 ± 0.02	0.45 ± 0.06
	τ (min)	36.3 ± 0.2	5.1 ± 0.1	80.7 ± 0.5
	R^2	0.9945	0.9972	0.9943

PFO: pseudo-first order; PSO: pseudo-second order; IDM: intraparticle diffusion model; MSR/DCK: mixed surface reaction and diffusion-controlled kinetic model.

where k_2 is the PSO adsorption rate constant, and θ_e and θ_t are the amount of PCM adsorbed at equilibrium and at a given time, respectively. The sorption rate can be calculated as the initial sorption rate when t approaches 0. Integration of Eq. (3) gives:

$$\frac{t}{\theta_t} = \frac{1}{k_2{\theta_e}^2} + \frac{t}{\theta_e} \tag{3}$$

where k_2 is the PSO rate constant and θ_e is the equilibrium adsorption capacity. $k_2\theta_e$ was calculated using a linear approach. The plots of $\frac{t\theta_e}{\theta_t}$ versus time (t), for the bands centered at 900, 1261 and 867 cm^{-1}, are shown in Fig. 6 and S4.

The kinetic parameters for the PFO and the PSO rate equations are listed in Table 2. The determination coefficients of the PSO kinetic model indicate that this model matches the experimental behavior better than the PFO model.

Nevertheless, a deviation from linearity as a downward curvature at initial times was observed (inset of Fig. 6 and Fig. S4). An explanation of the deviation is addressed below.

3.3.3. Intraparticle diffusion model (IDM)

The intraparticle diffusion model is applicable when the rate-determining step is the mass transfer of adsorbate to the solid surface sites [38,39] and is described by the Eq. (4):

$$\frac{\theta_t}{\theta_e} = 1 - \frac{6}{\pi^2}\sum_{n=1}^{\infty}\frac{1}{n^2}\exp\left(-\frac{Dn^2\pi^2}{r^2}t\right) \tag{4}$$

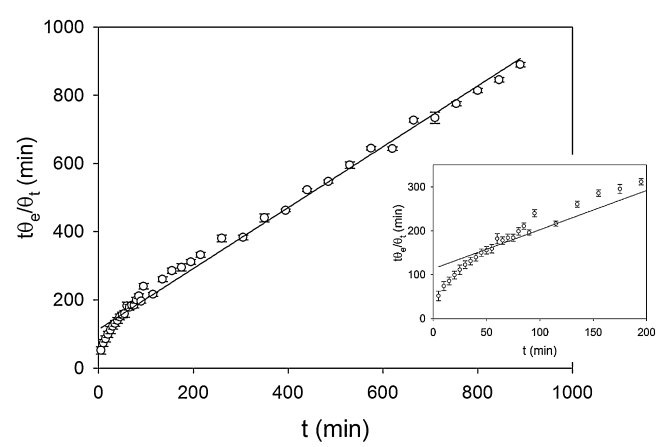

Fig. 6. Linear plot of t/θ_t versus time (t) for the band centered at 900 cm^{-1}. The solid line was obtained from Eq. (3) (PSO). The inset figure is included in order to clearly show the deviation from linearity as a downward curvature at initial times.

where D is the intraparticle diffusion coefficient and r is the particle radius. At short time, when the ratio between θ_t and θ_e is less than 0.3, the Eq. (4) can be reduced to

$$\theta_t = k_{id}\sqrt{t} \tag{5}$$

where k_{id} is the intraparticle diffusion constant.

Plots of $\frac{\theta_t}{\theta_e}$ at 1261, 900 or 867 cm^{-1} versus $t^{1/2}$, for PCM are shown in Fig. S5. The ratio between intra-particle diffusion rate k_{id} and θ_e was obtained from the slope from the linear regression of the curve (Table 2). The determination coefficients obtained were lower than 0.97, indicating that the intraparticle diffusion model was not the rate-controlling step of the PCM adsorption on Mt. The curves did not pass through the origin, which indicates that diffusion through the pores is not the limiting factor.

However, the deviation from linearity as a downward curvature at initial times when $\frac{t\theta_e}{\theta_t}$ versus t was plotted indicates that there is a contribution of the diffusion process to the rate-controlling step of adsorption as is observed in the insets of Fig. 6 and Fig. S4.

Haerifar and Azizian [37] have recently proposed that this behavior occurs when diffusion and surface reaction control the overall rate of the process at the solid/solution interface. In these cases, according to these authors, the mixed surface reaction and diffusion-controlled kinetic model (MSR/DCK) can be applied.

3.3.4. Mixed surface reaction and diffusion-controlled kinetic model (MSR/DCK)

The MSR/DCK model for adsorption kinetics has been recently reported by Haerifar and Azizian [37] and considers that diffusion contributes to the rate-controlling step of adsorption describing the experimental data better than the pure PSO model.

The MSR/DCK model considers that the adsorbate molecules diffuse toward the sorbent sites and then adsorb on the surface sites through a surface reaction mechanism.

The time dependence of the surface coverage has the following form:

$$\theta_t = \theta_e \frac{\exp(at + bt^{1/2}) - 1}{u_{eq}\exp(at + bt^{1/2}) - 1} \tag{6}$$

where $a = kC_0(u_{eq} - 1)$; $b = 2kC_0\tau^{1/2}(u_{eq} - 1)$; $u_{eq} = 1 - \frac{C_{eq}}{C_0}$ is the relative equilibrium uptake ($0 \le u_{eq} \le 1$; $k = \frac{k'}{\gamma}$; $\gamma = \frac{C_0 - C_e}{\theta_{eq}}$; $k' = 4\pi r_0 D$) is the rate coefficient in the Wait equation proposed in 1957 for a second-order reaction [37]; r_0 is the radius of the reaction cage; $\tau = \frac{r_0^2}{\pi D}$ is the ratio of the length of the transient period and is related to the effect of diffusion on the global rate; and D is the diffusion coefficient of the adsorbate that diffuses from the bulk solution to the interface.

According to this model, the effect of diffusion was determined by the coefficient b (more especially by τ) and the effect of surface reaction by both a and b coefficients.

The ratio between surface coverage and surface coverage at equilibrium, θ_t/θ_e, for the adsorption of PCM on a Mt film was plotted versus t for the band centered at 900 cm^{-1} (Fig. 5) and for bands at 1261 and 867 cm^{-1} (Fig. S2) and modeled using Eq. (6); the parameters obtained are listed in Table 2. The predicted values obtained from Eq. (6) are represented as solid lines in Fig. 5 and Fig. S2. The determination coefficients obtained ranged between 0.9943 and 0.9972, which were similar than those obtained using the PSO model, nevertheless, as was explained before, the presence of a deviation from linearity as a downward curvature at initial times for PSO model, indicating that the use of PSO model in this system is disadvantageous. The low values of u_{eq} indicated that the values of C_{eq} and C_0 were very similar in agreement with the fact that the band at 1362 cm^{-1} corresponding to PCM in solution remained constant during the experiment. The values of k were in the same order of magnitude indicating that the monitoring of the adsorption kinetics can be carried out using the bands at 1261, 900 or 867 cm^{-1} and the values of τ are related to the linearity deviation at initial times when the experimental data are plotted as $\frac{t\theta_e}{\theta_t}$ versus t (Fig. 6 and Fig. S4).

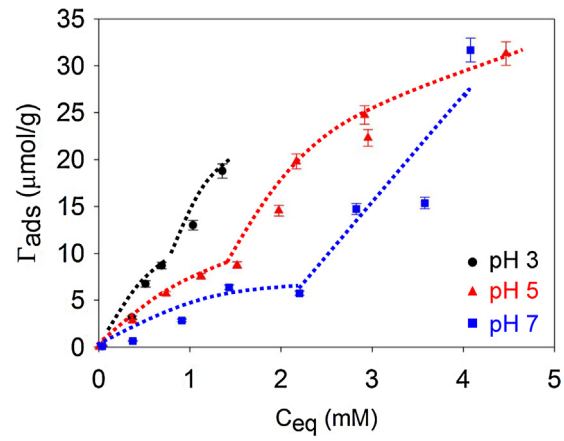

Fig. 7. PCM adsorption isotherms on Mt at indicated pH values. The dotted lines are placed on the graph as a guide to the eye.

3.4. Adsorption isotherms

The interactions of PCM with the clay mineral surfaces exhibited an anionic profile (Fig. 7), with a decrease in adsorption when the pH increases, which suggests that the adsorption of the PCM anion was coupled with a release of H_2O or OH^- ions. This behavior is in agreement with a coordination of the PCM molecule with surface sites with an interaction through pyridinic nitrogen and carboxylate groups by means of the formation of an inner sphere complex as indicated by FTIR results. Similar results have been reported before for PCM adsorption on a modified Mt with Fe oxides [19] and nitrate adsorption on biochars [40].

The adsorption of PCM by clay materials has been previously reported in very acidic systems [8], but for pH values greater than 3, the adsorption of PCM was not detected [11,18]. In the present work, it was observed that the PCM is considerably adsorbed onto Mt at pH values that were even greater than 3. Thus, PCM adsorption isotherms on Mt at pH 3, 5 and 7 are presented in Fig. 7.

Fig. 7 revealed an increase in the surface coverage (Γ_e) with C_{eq} after the adsorption *plateau*, which indicates the existence of successive adsorption processes over different surface active sites. The formation of the monolayer was completed at a certain value of C_{eq}, and when this concentration was attained, other sites contributed to the adsorption process [27].

The existence of two consecutive *plateaux* was attributed to two independent adsorption processes on different surface sites [27]. The first surface site could be associated with external and edge surfaces, and the second one with the interlayer surface. The first site was energetically more favorable than the second one, where PCM can also cause steric hindrance. The importance of both surface sites, which was previously mentioned, can be evidenced by normalizing Γ_e by the surface area using the S_{N2} value up to a C_{eq} where the formation of the first *plateau* was observed as well as the S_W value for higher values of C_{eq} [27].

Adsorption isotherms are important criteria for optimizing the use of adsorbent materials because they describe the nature of the interaction between the sorbate and the adsorbent. Thus, the analysis of the experimentally obtained equilibrium data using either theoretical or empirical equations is useful for the practical design and operation of adsorption systems. There are several

Table 3
Langmuir and Freundlich parameters for PCM adsorption on Mt at different pH values.

pH	Langmuir					Freundlich		
	pK_{L1} (L μmol^{-1})	pK_{L2} (L μmol^{-1})	Γ_{max1} (μmol m^{-2})	Γ_{max2} (μmol m^{-2})	R^2	$K_F \times 10^3$	$1/n$	R^2
3	2.75 ± 0.05	3.45 ± 0.04	0.54 ± 0.03	0.012 ± 0.004	0.9796	7.9 ± 0.3	0.55 ± 0.03	0.9324
5	2.92 ± 0.04	3.76 ± 0.03	0.45 ± 0.05	0.053 ± 0.004	0.9824	14.3 ± 0.4	0.41 ± 0.02	0.9271
7	3.22 ± 0.04	3.82 ± 0.05	0.34 ± 0.05	0.013 ± 0.005	0.9638	1.1 ± 0.5	0.66 ± 0.05	0.9611

The experimental error was less than 5% in all cases. K_{L1}: Langmuir equilibrium constant for the more reactive surface site; K_{L2}: Langmuir equilibrium constant for the less reactive surface site; Γ_{max1}: maximum uptake for the more reactive surface site; Γ_{max2}: maximum uptake for the less reactive surface site; K_F: Freundlich constant; $1/n$: an irrational fraction that varies between 0.1 and 1 and is a measure of the adsorption intensity.

expressions that describe adsorption isotherms; the Langmuir and the Freundlich models are the most widely applied expressions for the analyses of adsorption on all types of materials. Therefore, the experimental data for the adsorption of PCM were analyzed using both the Langmuir and Freundlich models.

3.4.1. Langmuir adsorption isotherms

The Langmuir isotherm quantitatively describes the growth of a monolayer of molecules on an adsorbent surface as a function of the concentration of the adsorbed material present in the liquid phase. This isotherm generally reveals a decrease in the number of available interaction sites as the concentration of the adsorbate increases. The Langmuir isotherm is represented by the following equation:

$$\Gamma_e = \frac{\Gamma_{max} K_L C_{eq}}{(1 + K_L C_{eq})} \quad (7)$$

where Γ_{max} is the maximum uptake and represents the maximum concentration that can be accumulated on the solid phase, C_{eq} is the adsorbate concentration at equilibrium in the aqueous solution, and K_L is the Langmuir equilibrium constant, which is related to the free energy of the reaction. The affinity between the sorbent and the sorbate is represented by this K_L constant. In general, for good sorbents, a high Γ_{max} and a high K_L are desirable.

The presence of two *plateaux* in the adsorption isotherms is considered in a two-term series Langmuir equation:

$$\Gamma_{ads} = \frac{\Gamma_{max\,1} K_{L1} C_{eq}}{(1 + K_{L1} C_{eq})} + \frac{\Gamma_{max\,2} K_{L2} C_{eq}}{(1 + K_{L2} C_{eq})} \quad (8)$$

where Γ_{max1} and K_{L1} are the parameters for the more reactive surface site and Γ_{max2} and K_{L2} are the parameters for the less reactive surface site. The total maximum uptake, Γ_{max}, is defined as the sum of the partial surface coverages ($\Gamma_{max} = \Gamma_{max1} + \Gamma_{max2}$). The parameters of the two-site Langmuir model and their determination coefficient (R^2) values are listed in Table 3.

3.4.2. Freundlich adsorption isotherms

The Freundlich isotherm is an empirical equation that describes the adsorption on a heterogeneous surface with a nonuniform distribution of heat of adsorption, which means that the surface where the adsorbed molecules are interacting is energetically heterogeneous. This model does not predict any saturation of the adsorbent by the adsorbate, but infinite surface coverage is predicted, which indicates the presence of multilayer adsorption on the surface. This isotherm is represented by Eq. (9).

Here, K_F is the Freundlich constant that indicates the adsorption capacity and represents a measure of the surface area of the adsorbent, and $1/n$ is an irrational fraction that varies between 0.1 and 1 and is a measure of the adsorption intensity.

Linear regression analysis was applied for the analysis of the isotherm data. The linear form of the Freundlich isotherm used was

$$\ln \Gamma_e = \ln K_F + \frac{1}{n} \ln C_{eq} \quad (9)$$

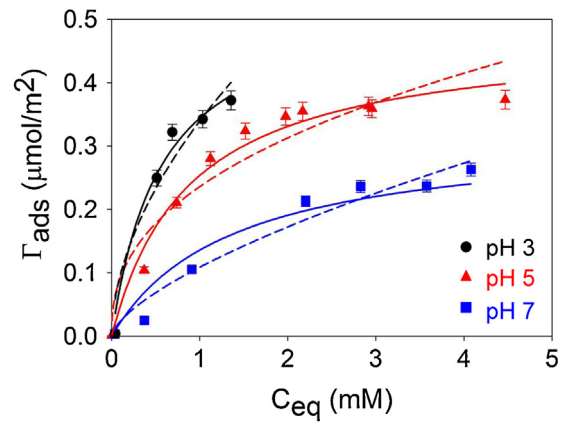

Fig. 8. PCM adsorption isotherms on Mt at indicated pH values. The solid and dotted lines were obtained from Eqs. (8) and (9) using the two-site Langmuir and Freundlich models, respectively.

K_F and $1/n$ were calculated from the intercept and slope of the plot between $\ln \Gamma_e$ vs $\ln C_{eq}$.

The K_F, $1/n$ and the R^2 values for the Freundlich isotherm parameters are given in Table 3.

Table 3 The PCM adsorption isotherms on Mt after normalization of Γ_e by the surface area and their fit to the Langmuir and Freundlich models are shown in Fig. 8. The solid lines in Fig. 8 are the two sites of the Langmuir model applied to the PCM uptake during the adsorption process; the calculated lines and the experimental data match very well with R^2 values between 0.9577 and 0.9824. The dotted lines represent the applied Freundlich model. Although the R^2 values for the Freundlich equation are acceptable, the Langmuir equation presented a better fit to the experimental results.

Recently, Freundlich constant values, K_F, of 1016.40 and $1/n$ value of 0.89 for the adsorption of PCM onto Mt and K_F, of 1.17 and a $1/n$ value of 0.93 for bentonite were reported [41]. Nevertheless, the methodology used in their study did not include a pH equilibration of the samples, the source and characterization of the Mt were not mentioned, the adsorption isotherms were not shown, and no adsorption *plateaux* were reported; therefore, a comparison with the data of Mt of this paper cannot be directly performed. However, the Freundlich parameters estimated in the present work where Γ_e and C_{eq} are expressed in the same units as those used by Fast et al. [41] are far from the parameters of Mt and similar to those obtained for bentonite.

4. Conclusions

This first adsorption kinetic study of an herbicide (PCM) onto montmorillonite (Mt) was done in situ using an ATR-FTIR method.

Mixed surface reaction intraparticle diffusion-controlled kinetic was the model that best represented the experimental results. The adsorption equilibrium isotherms revealed the presence of two independent adsorption processes on different surface sites. A better agreement with Langmuir than with Freundlich model

equations was obtained. The affinity constants were calculated and they decrease with increasing pH.

Due to the anionic form of PCM, the adsorption onto the external clay mineral surface sites followed by the entrance of the PCM molecule into the Mt basal space in a less energetically favorable pathway was proposed.

The adsorption pH dependence indicated an anionic bonding mechanism of the PCM toward the Mt surface, and FTIR spectra suggest inner sphere complex formation through pyridinic nitrogen atom and carboxyl group coordination.

The PCM adsorption on Mt interfaces was fast and the mobility of PCM in natural environments due to its low solubility produced low adsorption coverage. Thus, the fate and bioavailability of this herbicide in soil systems will depend on the strength of the interaction and the contact time with the solid phases.

Consequently, a better knowledge of the interactions of pesticides with clay minerals may allow a more judicious selection of materials for water/wastewater treatment filters that significantly enhance the removal of organic xenobiotics, and will help designing materials for the controlled release of herbicides or for use as geochemical barriers for hazardous materials.

Acknowledgments

The authors acknowledge the Universidad de Buenos Aires (UBA) and Ministerio de Ciencia y Tecnología, Agencia Nacional de Promoción Científica y Tecnológica, Fondo para la Investigación Científica y Tecnológica (MINCyT-ANPCyT-FONCyT) for financial support through UBACyT X043, X067 and PICT 23-32678 grants. Authors are also thankful to Consejo Nacional de Investigaciones Científicas y Técnicas de la República Argentina (CONICET).

Appendix A. Supplementary data

Supplementary data associated with this article can be found, in the online version, at http://dx.doi.org/10.1016/j.colsurfa.2014.02.038.

References

[1] J. Zhang, B. Shi, T. Li, D. Wang, Adsorption of methyl parathion on PAC from natural waters: the effect of NOM on adsorption capacity and kinetics, Adsorption 19 (2013) 91–99.
[2] G. Palma, A. Sánchez, Y. Olave, F. Encina, R. Palma, R. Barra, Pesticide levels in surface waters in an agricultural-forestry basin in Southern Chile, Chemosphere 57 (2004) 763–770.
[3] O.P. Bansal, Fate of pesticides in the environment, J. Indian Chem. Soc. 88 (2011) 1525–1532.
[4] M. Loewy, V. Kirs, G. Carvajal, Groundwater contamination by azinphos methyl in the Northern Patagonic Region, Sci. Total Environ. 225 (1999) 211–218.
[5] Food and Agriculture Organization of the United Nations (2007), FAO Specifications and evaluations for Agricultural Pesticides, Picloram, http://www.fao.org
[6] T.L. Lavy, J.D. Mattice, J.H. Massey, B.W. Skulman, S.A. Senseman Jr., E.E. Gbur, M.R. Barrett, Long-term in situ leaching and degradation of six herbicides aged in subsoils, J. Environ. Qual. 25 (1996) 1268–1279.
[7] M. Cheung, J. Biggar, Solubility and molecular structure of 4-amino-3,5,6-trichloropicolinic acid in relation to pH and temperature, J. Agr. Food Chem. 22 (1974) 202–206.
[8] J. Biggar, U. Mingelgrin, M. Cheung, Equilibrium and kinetics of adsorption of picloram and parathion with soils, J. Agr. Food Chem. 26 (1978) 1306–1312.
[9] R.W. Bovey, C.W. Richardson, Organic chemicals in the environment: dissipation of clopyralid and picloram in soil and seep flow in the backlands of texas, J. Environ. Qual. 20 (1991) 528–531.
[10] A.J. Krzyszowska, R.D. Allen, G.F. Vance, Assessment of the fate of two herbicides in a Wyoming rangeland soil: Column studies, J. Environ. Qual. 23 (1994) 1051–1058.
[11] R. Celis, M. Hermosín, L. Cornejo, M. Carrizosa, J. Cornejo, Clay-herbicide complexes to retard picloram leaching in soil, Int. J. Environ. Anal. Chem. 82 (2002) 503–517.
[12] M.E. Close, G.N. Magesan, R. Lee, M.K. Stewart, J.C. Hadfield, Field study of pesticide leaching in an allophanic soil in New Zealand. 1: Experimental results, Aust. J. Soil Res. 41 (2003) 809–824.
[13] T.Y. Kim, S.S. Park, S.S.Y. Cho, Separation characteristics of some phenoxy herbicides from aqueous solution, Adsorption 14 (2008) 611–619.
[14] N. Sahiner, S. Butun, P. Ilgin, Hydrogel particles with core shell morphology for versatile applications: environmental, biomedical and catalysis, Colloids Surf. A 386 (2011) 16–24.
[15] I. Pavlovic, C. Barriga, M. Hermosín, J. Cornejo, J. Ulibarri, Adsorption of acidic pesticides 2,4-D, clopyralid and picloram on calcined hydrotalcite, Appl. Clay Sci. 30 (2005) 25–33.
[16] A.G.S. Prado, A.H. Tosta, C. Airoldi, Adsorption, separation, and thermochemical data on the herbicide picloram anchored on silica gel and its cation interaction behavior, J. Colloid Interface Sci. 269 (2004) 259–264.
[17] J.L. Marco-Brown, C.M. Barbosa-Lema, R.M. Torres Sánchez, R.C. Mercader, M. dos Santos Afonso, Adsorption of picloram herbicide on iron oxide pillared montmorillonite, Appl. Clay Sci. 58 (2012) 25–33.
[18] R. Grover, Adsorption of picloram by soil colloids and various other adsorbents, Weed Sci. 19 (1971) 417–418.
[19] W. Farmer, Y. Aochi, Picloram sorption by soils, Proc. Soil Sci. Soc. Am. 38 (1974) 418–423.
[20] Y. Coquet, Variation of pesticide sorption isotherm in soil at the catchment scale, Pest Manag. Sci. 58 (2002) 69–78.
[21] A. El Arfaoui, S. Sayen, M. Paris, A. Keziou, M. Couderchet, E. Guillon, Is organic matter alone sufficient to predict isoproturon sorption in calcareous soils? Sci. Total Environ. 432 (2012) 251–256.
[22] N. Rauf, S.S. Tahir, J-H. Kang, Y-S. Chang, Equilibrium, thermodynamics and kinetics studies for the removal of alpha and beta endosulfan by adsorption onto bentonite clay, Chem. Eng. J. 192 (2012) 369–376.
[23] F. Barbier, G. Duc, M. Petit-Ramel, Adsorption of lead and cadmium ions from aqueous solution to the montmorillonite/water interface, Colloids Surf. A 166 (2000) 153–159.
[24] M.E. Parolo, M.J. Avena, M.C. Savini, M.T. Baschini, V. Nicotra, Adsorption and circular dichroism of tetracycline on sodium and calcium-montmorillonites, Colloids Surf. A 417 (2013) 57–64.
[25] B. Lombardi, R.M. Torres Sánchez, P. Eloy, M. Genet, Interaction of thiabendazole and benzimidazole with Montmorillonite, Appl. Clay Sci. 33 (2006) 59–65.
[26] R.M. Torres Sánchez, M.J. Genet, E.M. Gaigneaux, M. dos Santos Afonso, S. Yunes, Benzimidazole adsorption on the external and interlayer surfaces of raw and treated Montmorillonite, Appl. Clay Sci. 53 (2011) 366–373.
[27] G.A. Khoury, T.C. Gehris, L. Tribe, R.M. Torres Sánchez, M. dos Santos Afonso, Glyphosate adsorption on montmorillonite: an experimental and theoretical study of surface complexes, Appl. Clay Sci. 50 (2010) 167–175.
[28] L. Wang, J. Zhang, A. Wang, Removal of methylene blue from aqueous solution using chitosan-g-poly(acrylic acid)/montmorillonite superadsorbent nanocomposite, Colloids Surf. A 322 (2008) 47–53.
[29] P. Roonasi, A. Holmgren, An ATR-FTIR study of sulphate sorption on magnetite: rate of adsorption, surface speciation, and effect of calcium ions, J. Colloid Interface Sci. 333 (2009) 27–32.
[30] J.L. Marco-Brown., Adsorción de Picloram sobre Minerales Arcillosos, Ph.D. Dissertation, Buenos Aires University, 2011.
[31] M. Tschapek, R.M. Torres Sánchez, C. Wasowski, Handy methods for determining the isoelectric point of soils, Z. Pfla. Boden. 152 (1989) 73–76.
[32] D. Siguin, S. Ferreira, L. Froufe, F. García, Smectites, the relation-ship between their properties and isomorphic substitution, J. Mater. Sci. 29 (1994) 4379–4384.
[33] L.J. Michot, F. Villieras, Surface area and porosity, in: F. Bergaya, B.K. Theng, G. Lagaly (Eds.), Handbook of Clay Science. Developments in Clay Science, Elsevier, Amsterdam, 2006, pp. 965–978.
[34] E. Bojemueller, A. Nennemann, G. Lagaly, Enhanced pesticide adsorption by thermally modified bentonites, Appl. Clay Sci. 18 (2001) 277–284.
[35] A. Magnoli, L. Tallone, C. Rosa, A.M. Dalcero, S.M. Chiacchiera, R.M. Torres Sánchez, Commercial bentonites as detoxifier as broiler feed contaminated with aflatoxinas, Appl. Clay Sci. 40 (2008) 63–71.
[36] J.S. Loring, M. Karlsson, W.R. Fawcett, W.H. Casey, Attenuated total reflection–Fourier-transform infrared and ^{27}Al–nuclear magnetic resonance investigation of speciation and complexation in aqueous Al(III)–picolinate solutions, Geochim. Cosmochim. Acta 64 (2000) 4115–4129.
[37] M. Haerifar, S. Azizian, Mixed surface reaction and diffusion-controlled kinetic model for adsorption at the solid/solution Interface, J. Phys. Chem. C 117 (2013) 8310–8317.
[38] M.M. Areco, L. Saleh-Medina, M.A. Trinelli, J.L. Marco-Brown, M. dos Santos Afonso, Adsorption of Cu(II), Zn(II), Cd(II) and Pb(II) by dead *Avena fatua* biomass and the effect of these metals on their growth, Colloids Surf. B. 110 (2013) 305–312.
[39] A.K. Bhattacharya, C. Venkobachar, Removal of cadmium (II) by low cost adsorbents, J. Environ. Eng. 110 (1984) 110–122.
[40] R. Chintala, J. Mollinedo, T.E. Schumacher, D.D. Malo, S. Papiernik, D.E. Clay, S. Kumar, D.W. Gulbrandson, Nitrate sorption and desorption by biochars produced from microwave pyrolysis, Microporous and Mesoporous Mater. 179 (2013) 250–257.
[41] B.J. Fast, J.A. Ferrell, G.E. MacDonald, L.J. Krutz, W.N. Kline, Picloram and aminopyralid sorption to soil and clay minerals, Weed Sci. 58 (2010) 484–489.